https://doi.org/10.1038/s44431-025-00014-5

Sharp subthreshold switching in interface-modified organic electrochemical transistors for millivolt-level signal sensing

Hanyu Sun[1,2], Masaki Ishii[1,3], Jun Takeya[1,2], Katsuhiko Ariga[1,2,3] ✉ & Yu Yamashita[1,2] ✉

Organic electrochemical transistors (OECTs) are emerging as promising platforms for low-voltage bioelectronics applications. However, the use of sharp switching behavior for sensing has remained a challenge due to effects of structural disorders and operational stability. In this study, we report OECTs with subthreshold swings close to or even below the thermodynamic limit of 60 mV dec^{-1}. The sharp switching owe to the semicrystalline nature of the employed thin films showing reversible dopant ion intercalation responding to the gate bias. Furthermore, the introduction of a Langmuir-Blodgett amphiphilic membrane at the semiconductor-electrolyte interface effectively suppressed performance drift. The drift in threshold voltage was as small as 0.18 mV per hour, enabling the use of subthreshold regions for sensing applications. By leveraging the pH-responsivity of the functional monolayer, pH sensing was demonstrated. This work demonstrates benchmark switching performance and stability of OECTs, and the potential of supramolecular interface engineering for sensing platforms.

Organic electrochemical transistors (OECTs) have emerged as versatile mixed ionic-electronic transducers, offering low-voltage operation, mechanical flexibility, and coupling between ionic and electronic processes[1–5]. In contrast to conventional field-effect transistors, OECTs operate via electrochemical doping, introducing carriers and ions into the conjugated polymer active materials. This enables large conductance and current modulation with small gate-voltage inputs[6], which make OECTs highly suitable for chemical and biological sensing, particularly for in situ signal amplification under physiological conditions[7–9]. Ionic-electronic transduction by OECTs is also used to emulate synaptic behavior for analog signal processing and brain-inspired computing[10,11]. These features position OECTs as a promising platform for next-generation bioelectronics applications.

To achieve highly sensitive operation, the use of the subthreshold region is advantageous. Subthreshold swing (SS) is defined as the required voltage to change the current by one order of magnitude in the subthreshold region and serves as a critical parameter for evaluating the switching sharpness of a transistor. Small SS contributes to signal amplification and low-voltage device operation. In OECTs, structural disorders often result in large SS values, typically in the range of 100–150 mV dec^{-1}, which significantly exceeds the theoretical thermal limit of ~ 60 mV dec^{-1} at room temperature[12,13]. To achieve small SS, the choice of polymeric semiconductor is a crucial factor. Side chain engineered polymers with ordered structures with capability of volumetric ion doping, have been demonstrated to realize SS close to 60 mV dec^{-1}[14]. Recently reported vertical OECTs can achieve SS values as low as 60–65 mV dec^{-1} [15]. However, the active material is not adjacent to the electrolyte, which may not be suitable for sensing applications.

Another persistent challenge lies in the operational stability of OECTs, particularly with respect to threshold voltage drift (V_{th}) under aqueous environments, which can significantly compromise long-term device reliability and the accuracy of sensing performance. Importantly, the achievable detection limit of a sensor is determined by its sensitivity, noise level, and signal drift. OECT outputs tend to drift over time as the threshold voltage gradually shifts. This drift has been attributed to structural changes resulting from volumetric ion doping, where morphological deformation in disordered regions may be unavoidable. Such drift can obscure the detection of target analytes in biosensors and necessitate frequent recalibration.

[1]Research Center for Materials Nanoarchitectonics (MANA), National Institute for Materials Science (NIMS), Ibaraki, Japan. [2]Department of Advanced Materials Science, Graduate School of Frontier Sciences, The University of Tokyo, Chiba, Japan. [3]Graduate School of Science and Technology, Tokyo University of Science, Chiba, Japan. ✉e-mail: ARIGA.Katsuhiko@nims.go.jp; YAMASHITA.Yu@nims.go.jp

Recent studies have reported various strategies to improve OECT stability, such as molecular design, chemical doping, material purification, achieving V_{th} drifts of several mV h^{-1} or higher under continuous operation as summarized in Table 1. Despite these advances, maintaining both low SS and minimal V_{th} drift in aqueous environments remains challenging. In the case of single-crystal organic semiconductors, their intrinsically stable molecular packing has been shown to result in minimal threshold voltage drift, comparable to that observed in commonly used Ag/AgCl reference electrodes[16]. In addition to bulk structural changes, both chemical and physical adsorption at the semiconductor-electrolyte interface are known contributors to drift, even in structurally robust materials such as silicon and other inorganic semiconductors[17–20]. Therefore, the design of thin-film and interface materials will be essential for achieving high operational stability without compromising device sensitivity. In this context, the use of molecularly engineered interfacial layers, including amphiphilic units[21,22], may provide significant advantages. The introduction of hydrophilic surfaces has been recognized as a general strategy to improve the operational stability of sensor devices by suppressing the non-specific adsorption of contaminants that occurs through hydrophobic interactions[23,24]. For transistors with extended-gate architectures, monolayer modification of the gate electrode surface has been widely employed to achieve diverse sensing functionalities[25]. In contrast, for OECT active polymers, where chemisorption of monolayers is more challenging than on gate electrodes, the integration of self-assembled monolayers[26] may offer a facile and effective route for interface modification, although this approach remains relatively unexplored.

Table 1 | Comparison of subthreshold swings and threshold voltage drifts in OECTs

Active material	SS (mV dec^{-1})	V_{th} drift (mV h^{-1})
PII2T-Si[42]	≈100	0.83
p(g2T-TT)[43]	≈60	7.8
IDTBT[44]	≈200	9.3
p(g3T2)[5]	≈100	25
LB-modified PBTTT (this work)	40-60	0.18

In this study, we report the development of OECTs based on the semicrystalline polymeric semiconductor poly(2,5-bis(3-tetradecylthiophen-2-yl)thieno[3,2-*b*]thiophene) (PBTTT[27]) doped with bis(trifluoromethanesulfonyl)imide (TFSI) anion (Fig. 1a). During OECT operation in aqueous electrolytes, we achieved an sharp subthreshold switching behavior approaching the thermodynamic limit of 60 mV dec^{-1}. To further enhance device stability and functionality, a fatty acid monolayer was introduced onto the OECT channel via the Langmuir-Blodgett (LB) method, with the hydrophilic headgroups oriented toward the aqueous phase. The resulting devices exhibit a remarkably low threshold voltage drift of only 0.18 mV h^{-1} under continuous operation in aqueous environments, exceeding the long-term stability of most previously reported OECTs (Fig. 2c). In addition to suppressing drift by stabilizing interfacial charge distributions, the monolayer imparts proton sensitivity, enabling reliable pH detection. These findings underscore the potential of combining semicrystalline polymeric semiconductors with molecular-level interfacial engineering to develop OECT-based platforms for high-performance, low-power, and stable chemical sensing applications.

Results

Surface-modified Organic Electrochemical Transistors

OECTs were fabricated by integrating a semicrystalline polymeric semiconductor with a molecularly defined interfacial modification layer. PBTTT was chosen as the active material due to its semicrystalline lamellar structure. The conjugated backbone forms π-π stacking in the horizontal plane, while the interdigitated alkyl side chains stack in the vertical direction[28]. This

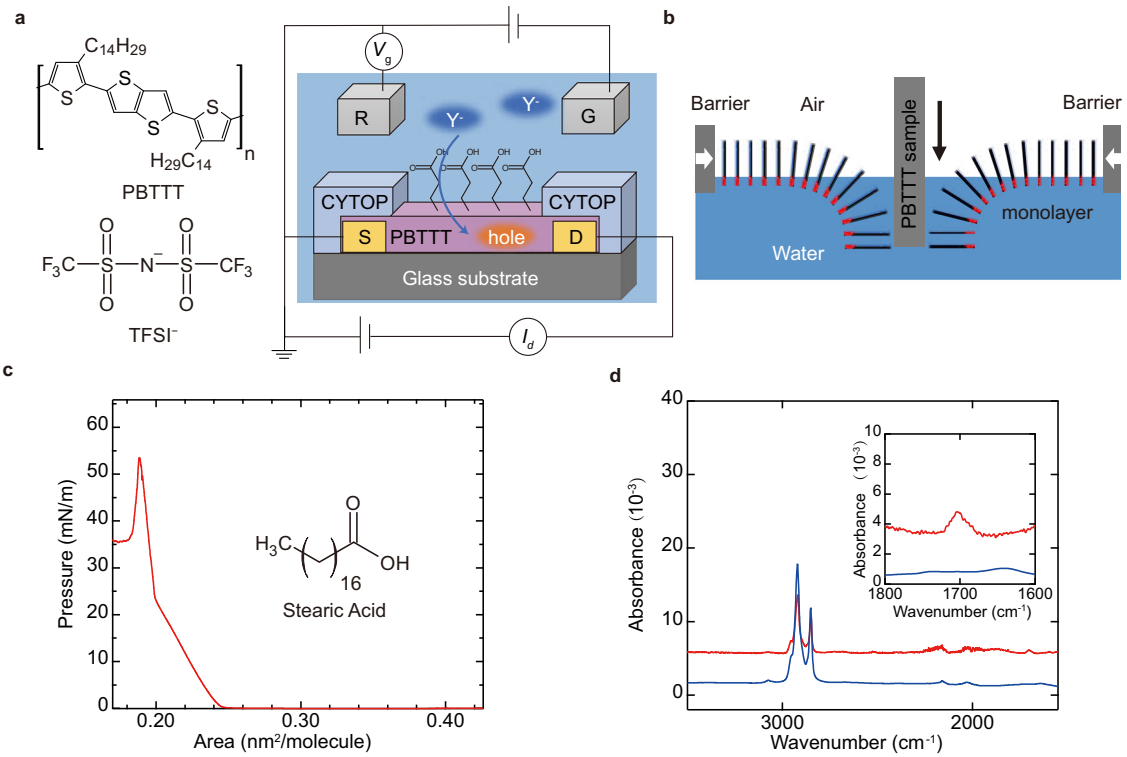

Fig. 1 | Fabrication of surface-modified OECTs. a Schematic of the surface-modified OECT with a lateral channel configuration using PBTTT as the semiconductor and a LB fatty acid monolayer as the interfacial layer. **b** Illustration of the LB deposition process. Stearic acid molecules form a monolayer at the air-water interface and are subsequently transferred onto the PBTTT surface via vertical immersion. **c** π-A isotherm of the stearic acid monolayer, showing a gas-to-condensed phase transition during compression. **d** The FT-IR spectrum of the PBTTT thin film before (blue) and after (red) transfer of the stearic acid monolayer. The inset shows a C=O stretching band at ~ 1700 cm^{-1}.

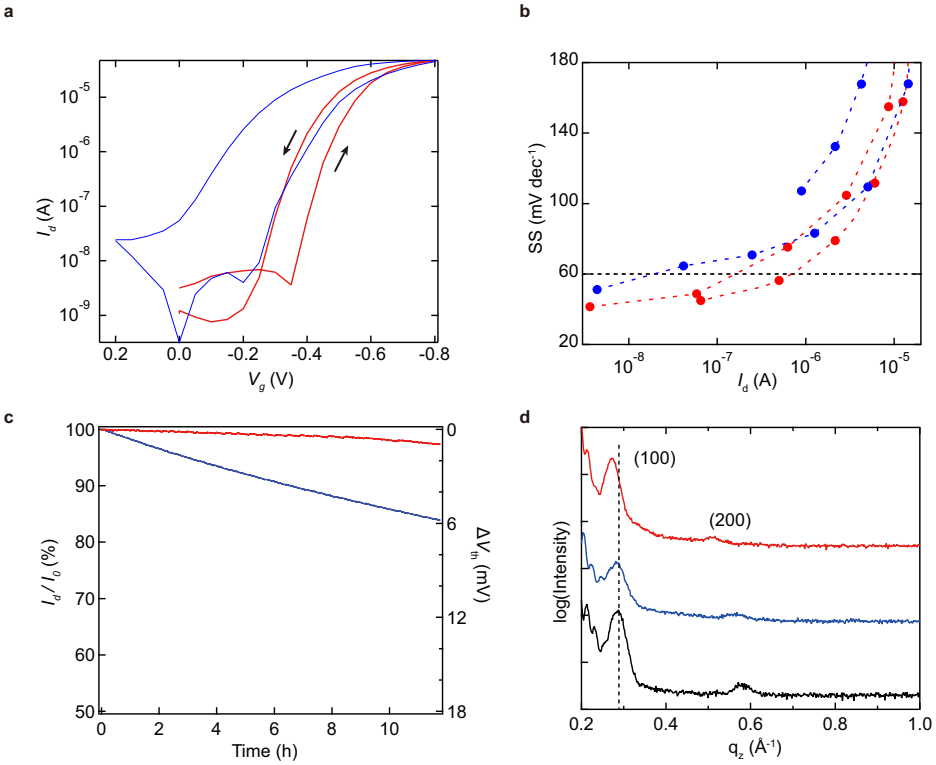

Fig. 2 | Electrical and structural characterizations of OECTs. a Transfer characteristics of OECTs with (red curve) and without (blue curve) the LB layer. V_d was − 0.01 V and V_g was swept by 0.05 V per 15 min. **b** SS extracted as a function of I_d for the devices with (red plot) and without (blue plot) the LB layer. **c** Operational stability of the OECTs under V_g of − 0.475 V and V_d of − 0.01 V for the devices with (red curve) and without (blue curve) the LB layer. The right axis indicates the threshold voltage shift, calculated assuming an SS of 60 mV dec^{-1}. **d** Out-of-plane XRD spectra of OECTs before operation (pristine, black curve), after applying V_g of − 0.4 V for 1 h (doped, red curve), and after subsequent application of V_g of 0 V for 1 h (dedoped, blue curve).

ordered morphology enables high in-plane carrier mobility while maintaining solution processability. As shown in Fig. 1a, the OECTs adopt a lateral channel geometry (See Fig. S1 for details), and the PBTTT thin film was prepared by spin coating followed by thermal annealing. While amphiphilic side chains can enhance ion intercalation kinetics, achieving crystallinity comparable to that of PBTTT has remained challenging. Importantly, PBTTT thin films can be doped in aqueous solutions without disturbing the crystallinity[29], making them a valuable model system for investigating the fundamental properties of OECTs.

To engineer the surface of the OECTs, we employed the LB method[26] to deposit a monolayer of stearic acid. This method enables precise control over molecular organization at the air-water interface and allows its transfer onto solid surfaces. As illustrated in Fig. 1b, stearic acid was first spread on the water surface using a volatile organic solvent. After solvent evaporation, the molecules assembled into a monolayer, with the hydrophobic alkyl tails pointing away from the water and the hydrophilic carboxylic acid headgroups oriented toward the aqueous phase. The molecular packing behavior of the stearic acid monolayer was controlled by compressing the film with a movable barrier, and the process was characterized by recording the surface pressure-area (π-A) isotherm (Fig. 1c). The observed transition from a gas-like to a liquid-condensed phase with increasing surface pressure indicates the formation of a compact and coherent monolayer suitable for transfer. In this study, the monolayer was compressed at a constant surface pressure (~15 mN m^{-1}) during transfer onto the PBTTT surface via vertical immersion of the substrate, ensuring that the hydrophilic termini face outward toward the electrolyte. Successful transfer of the monolayer was further confirmed by Fourier-transform infrared (FTIR) spectroscopy (Fig. 1d). The spectra exhibited characteristic absorption bands at ~1700 cm^{-1}, corresponding to the C=O stretching vibration of the carboxylic acid group. This vibrational signature confirms the successful immobilization of the fatty acid monolayer on the PBTTT surface.

The electrical performance of the OECTs was evaluated using an aqueous electrolyte containing 100 mM $TFSI^-$ dissolved in phosphate buffer solution (pH 7). As shown in Fig. 2a, transfer characteristics were measured for OECTs with and without the LB-deposited stearic acid monolayer. The gate voltage (V_g) was applied via an Ag/AgCl reference electrode to reflect the effective gate voltage without contributions from the gate electrode/electrolyte interface. Owing to the combination of hydrophobic materials and aqueous electrolyte, the OECTs exhibited relatively slow response, and V_g was swept in 0.05 V per 15 min. Both devices exhibited typical p-type OECT behavior, where the application of a negative gate bias leads to hole accumulation and an increase in drain current (I_d). To quantify switching sharpness, the subthreshold swing (SS) was extracted from the logarithmic regime of the transfer curve and plotted as a function of I_d in Fig. 2b. In the subthreshold regime, both devices exhibited sharp switching slopes approaching the thermodynamic limit of 60 mV dec^{-1}. Notably, the surface-modified device showed a more consistently low SS, which is attributed to the suppression of hysteresis.

In addition to sharp subthreshold switching, long-term operational stability was evaluated by monitoring I_d under a constant effective gate voltage defined using Ag/AgCl (Fig. 2c). Specifically, V_g was maintained at −0.475 V, which falls within the subthreshold regime of the OECTs. The gate currents during these measurements are shown in Fig. S2. The unmodified device exhibited an I_d drift of approximately 2% h^{-1}, corresponding to a threshold voltage drift of 1.38 mV h^{-1}. Given that the SS was close to 60 mV dec^{-1}, even small shifts in threshold voltage result in significant current fluctuations. Since most sensing signals are interpreted as shifts in voltage, threshold voltage drift is a critical parameter for reliable operation. The OECT with the LB monolayer exhibited markedly improved stability, showing an I_d drift of only 0.1% h^{-1}, equivalent to a threshold voltage drift of 0.18 mV h^{-1}. This level of stability is comparable to that of commercial Ag/AgCl reference electrodes[30]. The substantial improvement in long-term stability is likely attributable to the presence of the LB monolayer, considering that hydrophilic surfaces are known to suppress fouling and undesirable physisorption, both of which can contribute to performance drift in aqueous environments. The SS and V_{th} are compared with the literatures in Table 1, which highlights the sharp and stable OECT operation in this study.

The observation of a small SS can be attributed to the intrinsic structural characteristics of PBTTT. To investigate structural changes induced by electrochemical doping, out-of-plane X-ray diffraction (XRD) measurements were performed on PBTTT thin films before and after doping

(Fig. 2d). The pristine PBTTT film exhibited sharp diffraction peaks corresponding to the (100) and (200) reflections of its lamellar structure, indicating a high degree of molecular ordering. The *d*-spacing derived from the (100) peak of the undoped film was 21.86 Å. Following the application of a gate voltage (V_g) of −0.4 V for 1 h, the sample was removed from the electrolyte and subjected to XRD measurement. The doped sample showed a noticeable shift of the (100) peak toward a lower scattering vector q_z, corresponding to an expansion of the lamellar spacing to 23.22 Å. This lattice expansion provides clear evidence of the intercalation of dopant anions between the lamellar layers. Another sample was doped under the same conditions and then dedoped by applying V_g = 0 V for 1 h. This dedoped sample exhibited a *d*-spacing of 22.19 Å, approaching that of the pristine state. These reversible changes confirm the stable incorporation and removal of $TFSI^-$ anions within the PBTTT matrix without inducing irreversible structural damage.

Such a reversible doping process contributes to the observed small SS and overall device stability. SS increased when PBTTT films were baked at 100 °C, which is lower than the typical annealing temperature of 180 °C (Figs. S3 and S4). This is consistent with previous studies showing that high crystallinity reduces structural and energetic disorders, thereby leading to sharper subthreshold characteristics[31,32]. Interestingly, the SS value appears to fall below 60 mV dec^{-1} in the device modified with the LB monolayer. This phenomenon cannot be explained by conventional transistor operation based on entropic effects alone, and enthalpic effects would need to be considered[33]. In our case, considering the structural changes upon doping, concerted effects, such as the enhancement of doping efficiency driven by structural changes upon doping, may be involved.

pH sensing performance of surface-modified OECTs

To explore additional functionalities beyond switching behavior and stability, we further investigated the application of surface-modified OECTs as pH sensors. The key enabler is the stearic acid monolayer introduced via LB deposition, which provides a chemically active interface capable of responding to environmental pH through the protonation and deprotonation of terminal carboxylic acid groups. As the interfacial layer undergoes reversible transitions between neutral (COOH) and negatively charged (COO^-) states depending on the solution pH, it modulates the local electrostatic environment at the semiconductor-electrolyte interface[34]. This possibly influences the local ion activities at the interface and thus alters the device characteristics.

To assess the sensing performance, the device was subjected to repeated pH cycling between pH 3 and pH 11, with I_d monitored at a fixed V_g (Fig. 3a). The device exhibited an increase in I_d upon decreasing the pH. The gated current during this measurement is shown in Fig. S5. The drain current difference (ΔI_d) under different pH conditions is presented in Fig. 3b. The measurement data without LB layer is shown in S6. As shown in Fig. 3b, the LB-modified device exhibits a noticeably larger ΔI_d and a corresponding negative shift in V_{th} compared with the unmodified one when pH is lowered from 11 to 3, indicating that the interfacial stearic-acid monolayer effectively transduces protonation-deprotonation events into electrical signals. Note that most of the pH response seems to occur between pH values 3 to 7 (Fig. S7), reflecting the pKa of stearic acid[35–37] (*ca.* 5). These results demonstrate that the device provides stable signal responses and good repeatability under pH variations. This behavior can be explained by changes in the interfacial charge distribution. At higher pH, the increased presence of negatively charged COO^- groups is expected to reduce the interfacial activity of $TFSI^-$, thereby shifting the device's threshold voltage. The threshold voltage shift was calculated to be 7.63 mV based on ΔI_d, assuming a subthreshold swing of 60 mV dec^{-1}. Owing to the stable operation of the OECTs, the error in V_{th} was close to 1 mV, enabling clear detection of the small signal and highlighting the high sensitivity and stability of the device in the subthreshold regime.

In addition, the device response to different ionic species was examined to assess potential cross-sensitivity. The LB-modified OECT showed a negligible response to K^+ but a noticeable current change in the presence of Mg^{2+} ions, consistent with prior reports of divalent-ion coordination with fatty-acid monolayers[38,39] (Fig. S8). Further exploration of interfacial monolayers based on our strategy may expand the range of detectable targets.

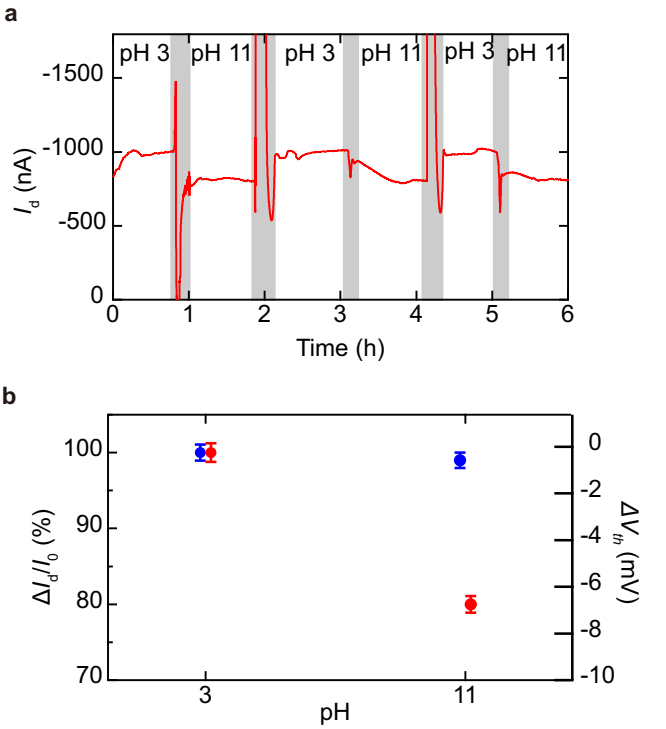

Fig. 3 | pH sensing performance of surface-modified OECTs. a Responses of I_d against pH changes between 3 and 11. V_d was − 0.01 V and V_g was − 0.475 V. The gray areas indicate the experimental operations to change the solution pH. **b** Changes in I_d and the corresponding threshold voltage shifts for the devices with (red markers) and without (blue markers) the LB layer. The threshold voltage shifts were calculated under the assumption of an SS of 60 mV dec^{-1}.

Discussion

Our findings demonstrate that OECTs incorporating semicrystalline polymer thin films and supramolecular interfacial modification exhibit improved SS and reduced V_{th} drift compared to previously reported devices, establishing a new performance benchmark and sensor platform for OECTs. However, the use of PBTTT with hydrophobic side chains resulted in a relatively slow response time (~30 min). Such timescales are still compatible with applications involving slowly varying chemical environments, such as long-term soil or water quality monitoring, for instance, in smart agriculture[40,41], where operational stability is prioritized over fast response. Further materials engineering will be required to enhance the response speed and broaden the applicability of the system.

In this work, we developed high-performance and stable OECTs by integrating the semicrystalline polymeric semiconductor PBTTT, doped with $TFSI^-$, and a molecularly engineered interfacial layer based on a Langmuir-Blodgett (LB) stearic acid monolayer. The PBTTT thin film, with its well-ordered lamellar structure and high crystallinity, enabled sharp subthreshold switching behavior close to the thermodynamic limit of 60 mV dec^{-1}. The introduction of the stearic acid monolayer further enhanced device performance by suppressing threshold voltage drift to as low as 0.18 mV h^{-1} under continuous aqueous operation-significantly surpassing the long-term stability of most reported OECTs. Furthermore, the interfacial monolayer functioned as a pH-responsive layer via reversible protonation and deprotonation of carboxylic acid groups, enabling reliable and repeatable proton sensing through modulation of electrochemical gating efficiency. An advantage of this supramolecular surface modification

is that it does not disrupt the crystallinity of the active channel material during the modification process. These results demonstrate that combining semicrystalline polymeric semiconductors with molecular-level interfacial engineering offers a viable strategy for constructing OECT-based platforms with low power consumption, high operational stability, and chemical sensing capability. This approach provides new insights into interfacial design for next-generation organic bioelectronics.

Methods

Materials

PBTTT (Mw > 50 000, SIGMA-ALDRICH, Co., Ltd.), stearic acid (GL Sciences Inc.), chloroform (Dojindo Molecular Technologies, Inc.), lithium bis(trifluoromethanesulfonyl) imide, and 1,2-dichlorobenzene(Tokyo Chemical Industry Co., Ltd.) were purchased and used without further purifications. Deionized water (18.2 MΩ · cm) was used in all LB experiments.

Device fabrication

OECTs with a lateral channel geometry were fabricated on glass substrates pre-patterned with gold source and drain electrodes. A 30-nm-thick layer of gold was deposited on the glass substrates as the electrodes by thermal evaporation. A thin film of PBTTT was spin-coated from a 1,2-dichlorobenzene solution (0.3 wt%) at 2000 rpm for 60 s, followed by thermal annealing at 180 °C in vacuum for 60 min. The channel length (L) was 500 μm and width (W) was 5500 μm.

LB monolayer deposition: Stearic acid (0.5 mg mL^{-1}) in chloroform was spread dropwise onto the surface of a Milli-Q water subphase in a LB trough. After solvent evaporation (15 min), the monolayer was compressed at a rate of 0.2 mm sec^{-1} to a target surface pressure of 15 mN m^{-1}. To transfer the LB monolayer, the PBTTT-coated substrate was vertically immersed through the monolayer at a speed of 0.02 mm sec^{-1} while keeping the surface pressure constant at 15 mN m^{-1}. Surface pressure-area isotherms were recorded during compression using a Wilhelmy plate.

Characterization

FTIR spectra were obtained using a Thermo Fisher Nicolet iS20 spectrometer in attenuated total reflectance (ATR) mode. Out-of-plane XRD measurements were performed on a Rigaku SmartLab diffractometer (Cu Kα, λ = 1.5406 Å). pH buffer solutions (pH 3 and pH 11) were prepared using standard buffer formulations. Transfer characteristics of the OECTs were measured in the buffer solution using an Keithley 2634B source measure unit, with Ag/AgCl reference and Pt gate electrodes. All of the V_g values in this paper are determined as the electrode potential difference between the Ag/AgCl electrode and source electrode connected to the ground. A typical output curve of our OECT is shown in Fig. S9.

Data availability

The data supporting this work are available in the main text and Supplementary Information.

Received: 30 June 2025; Accepted: 11 November 2025;
Published online: 07 January 2026

References

1. Rivnay, J. et al. Organic electrochemical transistors. *Nat. Rev. Mater.* **3**, 1–14 (2018).
2. Kergoat, L., Piro, B., Berggren, M., Horowitz, G. & Pham, M.-C. Advances in organic transistor-based biosensors: from organic electrochemical transistors to electrolyte-gated organic field-effect transistors. *Anal. Bioanal. Chem.* **402**, 1813–1826 (2012).
3. Khodagholy, D. et al. High transconductance organic electrochemical transistors. *Nat. Commun.* **4**, 2133 (2013).
4. Lan, L. et al. Side Chain Regioregularity Enables High-Performance and Sustainable Organic Electrochemical Transistors. *CCS Chem.* **7**, 1769–1782 (2025).
5. Le, V. N. et al. Improved organic electrochemical transistor stability using solvent degassing and chemical doping. *Nat. Electron.* **8**, 116–126 (2025).
6. Bernards, D. A. & Malliaras, G. G. Steady-state and transient behavior of organic electrochemical transistors. *Adv. Funct. Mater.* **17**, 3538–3544 (2007).
7. Sessolo, M., Rivnay, J., Bandiello, E., Malliaras, G. G. & Bolink, H. J. Ion-selective organic electrochemical transistors. *Adv. Mater.* **26**, 4803–4807 (2014).
8. Preziosi, V. et al. Organic electrochemical transistors as novel biosensing platforms to study the electrical response of whole blood and plasma. *J. Mater. Chem. B* **10**, 87–95 (2022).
9. Xie, K. et al. Organic electrochemical transistor arrays for real-time mapping of evoked neurotransmitter release in vivo. *eLife* **9**, e50345 (2020).
10. Van De Burgt, Y. et al. A non-volatile organic electrochemical device as a low-voltage artificial synapse for neuromorphic computing. *Nat. Mater.* **16**, 414–418 (2017).
11. He, W. et al. A facile membraneless method for detecting alkali-metal cations using organic electrochemical transistors. *J. Mater. Chem. C.* **12**, 18282–18290 (2024).
12. Hueting, R. J., Van Hemert, T., Kaleli, B., Wolters, R. A. & Schmitz, J. On Device Architectures, Subthreshold Swing, and Power Consumption of the Piezoelectric Field-Effect Transistor (π-FET). *IEEE J. Electron Devices Soc.* **3**, 149–157 (2015).
13. Wang, S. et al. An organic electrochemical transistor for multi-modal sensing, memory and processing. *Nat. Electron.* **6**, 281–291 (2023).
14. Giovannitti, A. et al. Controlling the mode of operation of organic transistors through side-chain engineering. *Proc. Natl. Acad. Sci.* **113**, 12017–12022 (2016).
15. Huang, W. et al. Vertical organic electrochemical transistors for complementary circuits. *Nature* **613**, 496–502 (2023).
16. Yamashita, Y. et al. Ion sensors based on organic semiconductors acting as quasi-reference electrodes. *Proc. Natl. Acad. Sci.* **121**, e2405933121 (2024).
17. Sasaki, Y. & Kawarada, H. Low drift and small hysteresis characteristics of diamond electrolyte-solution-gate FET. *J. Phys. D: Appl. Phys.* **43**, 374020 (2010).
18. Wei, W., Liao, W., Zeng, Z. & Zhu, C. Extended gate reference-FET (REFET) using 2D h-BN sensing layer for pH sensing applications. *IEEE Electron Device Lett.* **41**, 159–162 (2019).
19. Parish, G. et al. Role of GaN cap layer for reference electrode free AlGaN/GaN-based pH sensors. *Sens. Actuators B: Chem.* **287**, 250–257 (2019).
20. Jamasb, S., Collins, S. & Smith, R. L. A physical model for drift in pH ISFETs. *Sens. Actuators B: Chem.* **49**, 146–155 (1998).
21. Cui, M., Wang, Y., Wang, H., Wu, Y. & Luo, X. A label-free electrochemical DNA biosensor for breast cancer marker BRCA1 based on self-assembled antifouling peptide monolayer. *Sens. Actuators B: Chem.* **244**, 742–749 (2017).
22. Cui, M. et al. Mixed self-assembled aptamer and newly designed zwitterionic peptide as antifouling biosensing interface for electrochemical detection of alpha-fetoprotein. *ACS Sens.* **2**, 490–494 (2017).
23. Sutthiwanjampa, C., Hong, S., Kim, W. J., Kang, S. H. & Park, H. Hydrophilic modification strategies to enhance the surface biocompatibility of poly(dimethylsiloxane)-based biomaterials for medical applications. *Adv. Mater. Interfaces* **10**, 2202333 (2023).
24. Wang, X., Liu, Y., Cheng, H. & Ouyang, X. Surface wettability for skin-interfaced sensors and devices. *Adv. Funct. Mater.* **32**, 2200260 (2022).
25. Sasaki, Y. & Minami, T. Organic Transistor–Based Chemical Sensors for Real-Sample Analysis. *Phys. status solidi ((a))* **220**, 2300469 (2023).

26. Oliveira Jr, O. N., Caseli, L. & Ariga, K. The past and the future of Langmuir and Langmuir–Blodgett films. *Chem. Rev.* **122**, 6459–6513 (2022).
27. McCulloch, I. et al. Liquid-crystalline semiconducting polymers with high charge-carrier mobility. *Nat. Mater.* **5**, 328–333 (2006).
28. Cho, E. et al. Three-dimensional packing structure and electronic properties of biaxially oriented poly(2,5-bis(3-alkylthiophene-2-yl) thieno[3,2-*b*]thiophene) films. *J. Am. Chem. Soc.* **134**, 6177–6190 (2012).
29. Ishii, M., Yamashita, Y., Watanabe, S., Ariga, K. & Takeya, J. Doping of molecular semiconductors through proton-coupled electron transfer. *Nature* **622**, 285–291 (2023).
30. Mousavi, M. P., Saba, S. A., Anderson, E. L., Hillmyer, M. A. & Buhlmann, P. Avoiding Errors in Electrochemical Measurements: Effect of Frit Material on the Performance of Reference Electrodes with Porous Frit Junctions. *Anal. Chem.* **88**, 8706–8713 (2016).
31. Kalb, W. L. & Batlogg, B. Calculating the trap density of states in organic field-effect transistors from experiment: A comparison of different methods. *Phys. Rev. B* **81**, 035327 (2010).
32. Junpeng, Z. et al. Ultralow contact resistance in organic transistors via orbital hybridization. *Nat. Commun.* **14**, 324 (2023).
33. Bongartz, L. M. et al. Bistable organic electrochemical transistors: enthalpy vs. entropy. *Nat. Commun.* **15**, 6819 (2024).
34. Usui, S. & Healy, T. Zeta Potential of Stearic Acid Monolayer at the Air-Aqueous Solution Interface. *J. Colloid Interface Sci.* **250**, 371–378 (2002).
35. Quast, K. The use of zeta potential to investigate the pka of saturated fatty acids. *Adv. Powder Technol.* **27**, 207–214 (2016).
36. Škulj, S. & Vazdar, M. Calculation of apparent pka values of saturated fatty acids with different lengths in dopc phospholipid bilayers. *Phys. Chem. Chem. Phys.* **21**, 10052–10060 (2019).
37. Vysotsky, Y. B., Kartashynska, E. S. & Vollhardt, D. Surface pka of saturated carboxylic acids at the air/water interface: A quantum chemical approach. *J. Phys. Chem. C.* **124**, 13809–13818 (2020).
38. Brzozowska, A., Duits, M. & Mugele, F. Stability of stearic acid monolayers on artificial sea water. *Colloids Surf. A: Physicochemical Eng. Asp.* **407**, 38–48 (2012).
39. Diaz, M. E. & Cerro, R. L. On the effect of subphase ph and counterions on transfer ratios and dynamic contact angles during deposition of multiple langmuir-blodgett monolayers. *Thin Solid Films* **485**, 224–229 (2005).
40. Cho, W.-J. et al. On-site ion monitoring system for precision hydroponic nutrient management. *Computers Electron. Agriculture* **146**, 51–58 (2018).
41. Wu, S.-E. et al. Dual-gate organic electrochemical transistors for marine sensing. *Adv. Electron. Mater.* **7**, 2100223 (2021).
42. Knopfmacher, O. et al. Highly stable organic polymer field-effect transistor sensor for selective detection in the marine environment. *Nat. Commun.* **5**, 2954 (2014).
43. Venkatraman, V. et al. Subthreshold operation of organic electrochemical transistors for biosignal amplification. *Adv. Sci.* **5**, 1800453 (2018).
44. Simatos, D. et al. Electrolyte-gated organic field-effect transistors with high operational stability and lifetime in practical electrolytes. *SmartMat* **5**, e1291 (2024).

Acknowledgements

This work was supported in part by JSPS KAKENHI grants (no. JP25H00898). This work was supported in part by JST, CREST (no. JPMJCR21O3) and FOREST (no. JPMJFR236R). A part of this work was supported by "Advanced Research Infrastructure for Materials and Nanotechnology in Japan (ARIM)" of the Ministry of Education, Culture, Sports, Science and Technology (MEXT). Proposal Number JPMXP1225NM5259.

Author contributions

H.S. and M.I. performed the experiments and analyzed the data. K.A. and Y. Y. conceived of and designed the study. H.S. and Y.Y. wrote the manuscript. J.T. contributed to the discussion of electrical properties. All authors discussed the results and reviewed the manuscript.

Competing interests

The authors declare no competing interests.

Additional information

Supplementary information The online version contains supplementary material available at https://doi.org/10.1038/s44431-025-00014-5.

Correspondence and requests for materials should be addressed to Katsuhiko Ariga or Yu Yamashita.